the plant journal

SEB SOCIETY FOR EXPERIMENTAL BIOLOGY

The Plant Journal (2020) **103,** 1858–1868 doi: 10.1111/tpj.14873

CELLULOSE SYNTHASE INTERACTING 1 is required for wood mechanics and leaf morphology in aspen

Anne Bünder[1], Ola Sundman[2], Amir Mahboubi[3], Staffan Persson[4], Shawn D. Mansfield[5], Markus Rüggeberg[6,7] and Totte Niittylä[1,*]

[1]*Department of Forest Genetics and Plant Physiology, Umeå Plant Science Centre, Swedish University of Agricultural Sciences, Umeå, SE 901 83, Sweden,*

[2]*Department of Chemistry, Umeå University, Umeå, SE 901 87, Sweden,*

[3]*Department of Plant Physiology, Umeå Plant Science Centre, Umeå University, Umeå, SE 901 83, Sweden,*

[4]*School of Biosciences, University of Melbourne, Parkville, VIC, 3010, Australia,*

[5]*Department of Wood Science, University of British Columbia, Vancouver, BC, V6T 1Z4, Canada,*

[6]*Swiss Federal Institute of Technology Zurich (ETH Zurich), Institute for Building Materials, Zurich 8093, Switzerland, and*

[7]*Cellulose and Wood Materials, Swiss Federal Laboratories for Material Science and Technology (Empa), Dubendorf 8600, Switzerland*

Received 11 February 2020; revised 22 May 2020; accepted 1 June 2020; published online 11 June 2020.
*For correspondence (e-mail totte.niittyla@slu.se).

SUMMARY

Cellulose microfibrils synthesized by CELLULOSE SYNTHASE COMPLEXES (CSCs) are the main load-bearing polymers in wood. CELLULOSE SYNTHASE INTERACTING1 (CSI1) connects CSCs with cortical microtubules, which align with cellulose microfibrils. Mechanical properties of wood are dependent on cellulose microfibril alignment and structure in the cell walls, but the molecular mechanism(s) defining these features is unknown. Herein, we investigated the role of CSI1 in hybrid aspen (*Populus tremula* × *Populus tremuloides*) by characterizing transgenic lines with significantly reduced *CSI1* transcript abundance. Reduction in leaves (50–80%) caused leaf twisting and misshaped pavement cells, while reduction (70–90%) in developing xylem led to impaired mechanical wood properties evident as a decrease in the elastic modulus and rupture. X-ray diffraction measurements indicate that microfibril angle was not impacted by the altered *CSI1* abundance in developing wood fibres. Instead, the augmented wood phenotype of the transgenic trees was associated with a reduced cellulose degree of polymerization. These findings establish a function for CSI1 in wood mechanics and in defining leaf cell shape. Furthermore, the results imply that the microfibril angle in wood is defined by CSI1 independent mechanism(s).

Keywords: aspen, *Populus*, cell wall, wood mechanics, cellulose, transgenic trees, cellulose interacting 1, CSI1, pavement cell.

INTRODUCTION

Xylem supports the upright growth of trees, providing mechanical resistance against gravity and wind, and facilitates the effective transport of water and nutrients to aerial tissues of plants (Groover *et al.*, 2010). Xylem, or more commonly wood, is also a natural nanocomposite material, which potentiates sustainable applications that may drive a low carbon economy. The material and mechanical properties of wood is a function of the cellular architecture and the molecular interactions in the xylem cell walls. Wood of angiosperm trees consists of three main cell types. The water and nutrient transporting vessels, the ray cells involved in nutrient storage and radial transport, and the load-bearing xylem fibres that provide structural support (Groover *et al.*, 2010). Dimensions of fibres and wood density are important determinants of the mechanical properties of wood (Beery *et al.*, 1983), as is the angle at which cellulose microfibrils (CMFs) are laid down in the fibre walls (Evans and Elic, 2001; Barnett and Bonham, 2004). In wood, the CMFs are surrounded by heteropolysaccharide hemicelluloses and the complex phenolic lignin, which also are important for the mechanical performance of wood (Gibson, 1992). Understanding how wood formation and cell wall biosynthesis define the mechanical performance is a key aim in wood biology. Identification of the genes, the regulatory network and the master regulators of these processes are important and

relevant for tree breeding and biotechnological approaches focusing on improving the properties of timber and other wood-derived products.

Wood formation initiates in the cambial cell division zone. During cell expansion, the xylem fibre cell wall consists of a middle lamella between adjoining cells and a primary cell wall, which collectively combine to form the compound middle lamella. Plant cell expansion and the final cell dimensions are dictated by turgor-driven anisotropic extension of the primary cell wall, which largely depends on CMF orientation and their interactions with other matrix polymers (Cosgrove, 2005). In addition to anisotropic expansion, xylem fibres grow by intrusive tip growth where the tip of the cell grows in between neighbouring cells (Gorshkova *et al.*, 2012). Upon reaching their final size, xylem fibres initiate the synthesis of secondary cell walls, which at maturity typically contain two to three layers (Kerr and Bailey, 1934; Bailey and Vestal, 1937). The layer structure of the secondary fibre walls originates from altering orientation of the CMFs. The layers of the fibre secondary walls are classified as the outermost S_1 layer (adjacent to the primary wall), the middle S_2 layer representing the bulk of the total wall thickness, and the innermost S_3 layer (Harada, 1962; Fengel and Stoll, 1973; Fengel *et al.*, 1989). The mechanical properties of wood along the longitudinal fibre cell axis are particularly affected by the orientation of parallel CMFs in the S_2 layer (Preston, 1974).

The orientation of the CMFs in relation to the longitudinal axis of the fibre cell is defined as the cellulose microfibril angle (MFA). Generally, a low average MFA confers stiffness and strength to the wood, while a higher average MFA results in flexibility and toughness (Reiterer *et al.*, 2001). The molecular underpinnings defining the MFA in xylem fibres are not known, but immunofluorescence microscopy observations support a role for cortical microtubules (MTs) during both primary and secondary wall biosynthesis (Funada *et al.*, 1997; Barnett and Bonham, 2004). Immunostaining of developing xylem fibres using a tubulin antibody revealed parallel-arranged MTs, which were associated with secondary wall thickening in hybrid aspen (*Populus tremula* × *tremuloides*) and horse chestnut (*Aesculus hippocastanum*) (Chaffey *et al.*, 2000; Chaffey *et al.*, 2002). Chaffey *et al.* (2002) observed variation in MT orientation between neighbouring fibres undergoing secondary cell formation and hypothesized a connection to the different CMF alignments in the S_1, S_2 and S_3 layers. Experiments in Arabidopsis using MT-disrupting chemicals and MT defect mutants support a functional link between MTs and CMFs (Roberts *et al.*, 2004; Oda *et al.*, 2005; Wightman and Turner, 2008). Live cell imaging of fluorescent protein-tagged cellulose synthases (CESAs) in Arabidopsis established that cellulose synthase complexes (CSCs) track along the cortical MTs, which align with CMFs (Paredez *et al.*, 2006). This observation was made first during primary cell wall biosynthesis in etiolated hypocotyls and subsequently during secondary cell wall formation in protoxylem vessel-induced Arabidopsis seedlings (Paredez *et al.*, 2006; Wightman and Turner, 2008; Watanabe *et al.*, 2015; Li *et al.*, 2016; Watanabe *et al.*, 2018).

Genetic and protein interaction studies aimed at finding linker proteins between MTs and CSCs identified an armadillo/beta-catenin-like repeat containing protein called CELLULOSE SYNTHASE INTERACTING 1 (CSI1)/POM2) (Gu *et al.*, 2010). CSI1 can guide the CSCs along the cortical MTs during primary wall biosynthesis (Li *et al.*, 2012; Bringmann *et al.*, 2012a), and performs this function by interacting with both CSCs and MTs (Li *et al.*, 2012). Arabidopsis *csi1* mutants are impaired in cell expansion and display twisting epidermal cell files and leaves (Bringmann *et al.*, 2012b; Landrein *et al.*, 2013). Initial analysis of *csi1* mutants did not show defects in secondary cell walls (Gu and Somerville, 2010) but subsequently fluorescent CSC imaging established a role for CSI1/POM2 during the initial phase of secondary cell wall pattern establishment in xylem vessels (Schneider *et al.*, 2017).

CSI1 analyses during secondary cell wall biosynthesis have been limited to Arabidopsis xylem vessels, which lack the lamellar wall structure observed in xylem fibres. Here, we investigated the function of CSI1 in developing wood, and in particular xylem fibre formation in hybrid aspen (*Populus tremula* × *tremuloides*) using RNA interference of functional orthologues of the Arabidopsis *CSI1*.

RESULTS

Populus CSI1s are functional orthologues of the Arabidopsis CSI1

The *Populus* genome encodes two putative orthologues of the Arabidopsis CSI1 (Figure 1a). PtCSI1A and PtCSI1B are 95% similar to each other at the amino acid sequence level (Figure S1). To first test whether the *Populus* CSI1A can perform the same function as the Arabidopsis CSI1 we expressed the hybrid aspen (*Populus tremula* × *tremuloides*) *PttCSI1A* in the Arabidopsis *csi1* null mutant *pom2-4*. The *PttCSI1A* construct complemented the *pom2-4* silique and inflorescence length phenotypes confirming that PttCSI1A is indeed a functional orthologue of the Arabidopsis CSI1 (Figure S2). Based on publicly available transcriptome data, *PtCSI1A* and *PtCSI1B* are expressed in both leaves and stem (popgenie.org and http://aspwood.popgenie.org/aspwood-v3.0/). In the stem, the transcript abundance of both genes increase from cambium across the primary wall and cell expansion zone, peak at the onset of the secondary cell wall formation, and then decrease rapidly at the onset of cell death and xylem maturation (Figure 1b). Developing aspen wood also contains transcripts of the Arabidopsis *CSI3* homolog, but the transcript

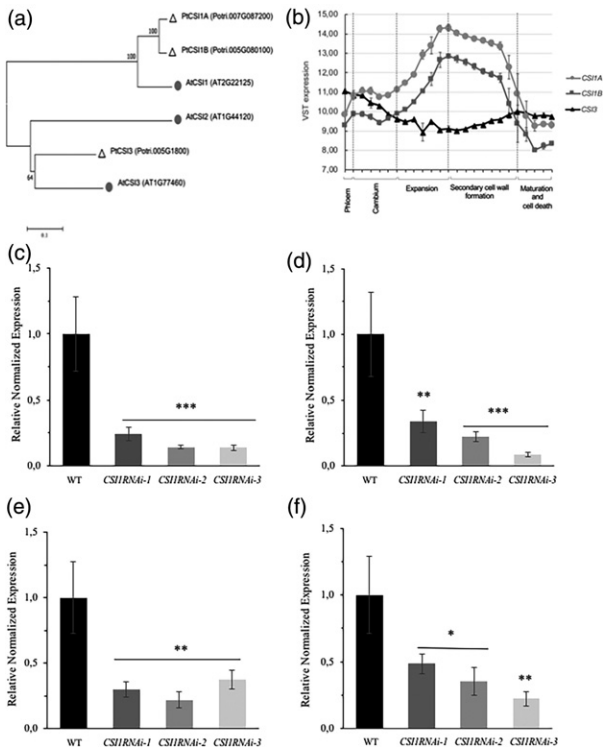

Figure 1. Aspen (*Populus tremula*) CSI family and genotyping of *CSI1RNAi* lines.
(a) Phylogenetic relationship of CSI amino acid sequences from aspen and *Arabidopsis thaliana*.
(b) Aspen *CSI1A*, *CSI1B* and *CSI3* transcript levels in phloem, cambium and different wood developmental zones. Data derived from http://aspwood.popgenie.org/aspwood-v3.0/.
Relative transcript abundance of wild-type (WT) and *CSI1RNAi* lines 1, 2 and 3: (c) *CSI1A* in developing wood, (d) *CSI1B* in developing wood, (e) *CSI1A* in leaves, (f) *CSI1B* in leaves. Error bars represent ± SD ($n = 4$ biological replicates). Asterisks indicate P values for comparison with WT: $*P < 0.05$; $**P < 0.01$; $***P < 0.001$ (Student's t-test). VST, variance-stabilizing transformation.

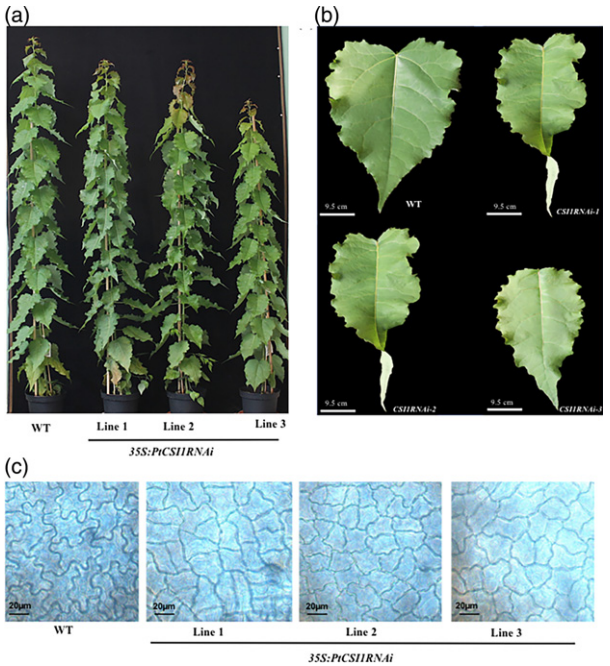

Figure 2. Phenotype of the wild-type (WT) and *CSI1RNAi* hybrid aspen (*Populus tremula* × *tremuloides*) lines.
(a) Two-month-old greenhouse grown WT and *CSI1RNAi* trees.
(b) Comparison of WT and *CSI1RNAi* leaves.
(c) Comparison of pavement cell shape in WT and *CSI1RNAi* leaf epidermis.

level does not show obvious changes during wood formation (Figure 1b). These developing wood transcript profiles suggested a function for PtCSI1A and PtCSI1B during xylem cell expansion and secondary cell wall formation. To study the role of *PttCSI1* in trees, transgenic hybrid aspen containing a 35S promoter driven *PttCSI1RNAi* construct targeting both *CSI1A* and *CSI1B* were generated and grown under greenhouse conditions for 2 months, to a height of approximately 1.5 m. Quantitative polymerase chain reaction (qPCR) analysis of *PttCSI1A* and *PttCSI1B* showed significant reduction in the transcript abundance of both genes in leaves and developing wood of three independent transgenic lines (Figure 1c–f).

CSI1RNAi causes leaf twisting and defects in pavement cell shape

The greenhouse grown *CSI1RNAi* lines showed a modest growth phenotype (Figure 2a). The average stem diameter was reduced in lines 1 and 3, and the stem height was slightly reduced in all transgenic lines (Table 1). The most obvious visual phenotype was a reduction in leaf size and the appearance of occasional twisting of the leaves (Figure 2b and Table 1). This was reminiscent of the twisting rosette leaves and other tissues observed in the Arabidopsis *csi1*/*pom2* null mutants (Bringmann *et al.*, 2012a; Landrein *et al.*, 2013). Interestingly, light microscopy inspection of the *CSI1RNAi* leaf epidermis revealed that the pavement cells lacked the multi-lobed jigsaw puzzle shape observed in the wild-type (WT) cells (Figure 2c). CMFs are known to mediate directional cell growth and the leaf epidermis plays an important role in defining leaf shape and size by bearing the stress caused by leaf growth. Hence, it seems likely that the leaf area reduction and twisting in the *CSI1RNAi* lines could be due to misaligned CMFs manifesting in defects in pavement cell and leaf shape formation.

CSI1RNAi wood is mechanically weaker

The phenotypic changes in the *CSI1RNAi* lines and the reduced *CSI1* transcript levels in the developing wood indicated that the *CSI1RNAi* lines could be used to investigate CSI1 function during wood formation and secondary growth. To this end, wood from WT, *CSI1RNAi* lines 1 and 3 was analysed in detail. Light microscopy of wood cross-

Table 1 Height, diameter 10 cm above the soil, and a fully expanded leaf area of wild-type (WT) and *CSI1RNAi* hybrid aspen (*Populus tremula* × *tremuloides*) lines at harvest

Line	Stem height (cm)	Stem diameter (mm)	Leaf area (cm^2)
WT	167 ± 3^{a}	6.8 ± 0.9^{a}	159 ± 17^{a}
CSI1RNAi-1	155 ± 7^{b}	6.3 ± 0.8^{ab}	97 ± 13^{b}
CSI1RNAi-2	157 ± 8^{b}	7 ± 1.3^{ab}	98 ± 12^{b}
CSI1RNAi-3	133 ± 4^{c}	6 ± 1.1^{b}	78 ± 14^{b}

Mean ± SD, $n = 6$ biological replicates. Means not sharing a common letter are significantly different at $P < 0.05$, as determined by Tukey's test after one-way ANOVA.

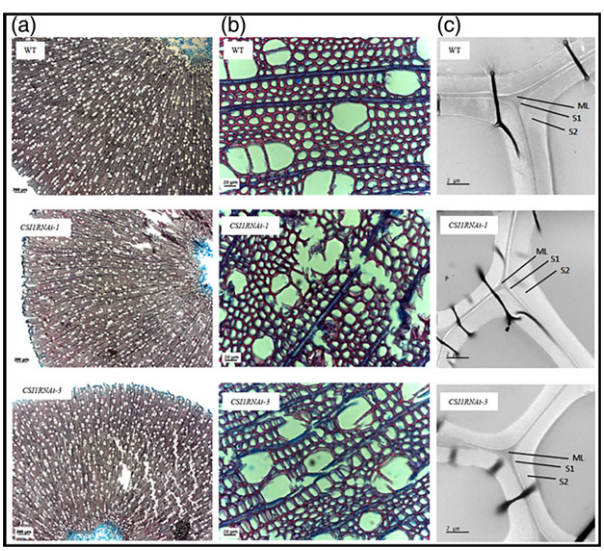

Figure 3. Wood anatomy in the wild-type (WT) and *CSI1RNAi* hybrid aspen (*Populus tremula* × *tremuloides*) lines.
(a,b) Light microscopy images of representative stem sections.
(c) Transmission electron microscopy images of representative mature wood fibre walls. Cell wall layers are indicated as middle lamella (ML), S_1 and S_2.

sections in the *CSI1RNAi* lines showed no obvious differences in the overall cellular anatomy among the transgenic lines and WT trees (Figure 3a). However, we observed that the 20-μm thick wood cross-sections derived from *CSI1RNAi* wood were more prone to cracking during sample preparation. The cracks occurred across the secondary cell walls of both fibres and vessels indicating that the mechanical integrity of the wall was affected in both cell types (Figure 3b). Transmission electron microscopy (TEM) was used to produce images of the secondary cell wall layer structure of xylem fibre walls, but no obvious changes in the thickness of the S_1 or S_2 layers or the structure of the fibre walls was observed (Figure 3c).

To examine the cell wall structure and mechanical properties further, we compared WT and *CSI1RNAi* wood in micromechanical tensile tests. Longitudinal–tangential wood strips with dimensions of 30 × 2 × 0.1 mm were strained to failure using a microtensile testing stage. The stiffness (modulus of elasticity, MOE) in longitudinal direction and the maximum force required to break the sample (modulus of rupture, MOR) were determined from the stress-strain curves. Significant differences were observed in both MOE and MOR between *PttCSI1RNAi* lines and WT trees. The MOE was reduced approximately by one-third, from 2.95 GPa in the WT to 2 GPa in the transgenics (Figure 4a). The MOR was also reduced in both lines although the difference was only significant for line 3 (Figure 4b).

CSI1RNAi wood density and average MFA are not changed

To investigate the origin of the observed mechanical weakness in *CSI1RNAi* wood we compared the cell wall composition in the transgenic lines and WT. No consistent differences were observed in lignin, cellulose or hemicellulosic sugar content (Table S2). These results indicated that the mechanical wood phenotype was not linked to changes in the composition of the cell wall matrix.

Based on the leaf twisting phenotype, the defects in the pavement cell shape and the CSI1 function in connecting CSCs and MTs, we hypothesized that the cellulose MFA could be affected in the *CSI1RNAi* wood. The average wood MFA of the S_2 layer of xylem fibre walls was determined using X-ray diffraction. Surprisingly, no consistent difference between WT and the transgenic lines was observed in normal wood (Table 2). In line 3, there was a tendency towards a slight MFA increase, but this was not statistically significant. The MFA agrees with those reported in the literature for the S_2 layer in juvenile wood of *Populus* sp. (Barnett and Bonham, 2004). We also sampled stem areas with apparent tension wood fibres and gelatinous layer (G-layer) formation where a bimodal orientation distribution of CMFs is seen with very small MFAs for the G-layers and larger angles (>30°) for the S_2 layer of tension wood (Müller *et al.*, 2006). However, this mechano-gravitropism induced MFA shift was near-identical between the WT and the *CSI1RNAi* lines (Table 2). These MFA results showed that the mechanical wood phenotype cannot be explained by a change in the orientation of the CMFs in the secondary cell wall layers, and indicated that CSI1 may not be needed for the alignment of CMFs during secondary cell formation in wood fibres in aspen trees.

CSI1RNAi reduced the xylem fibre area and the degree of cellulose polymerization

The longitudinal xylem fibre area measured from light microscopy images of macerated wood showed a consistent reduction by approximately 20% (Table 2). These data suggested that *CSI1RNAi* reduced the extent of fibre cell expansion. This is in line with the leaf data and suggested a defect during primary wall cellulose biosynthesis also in

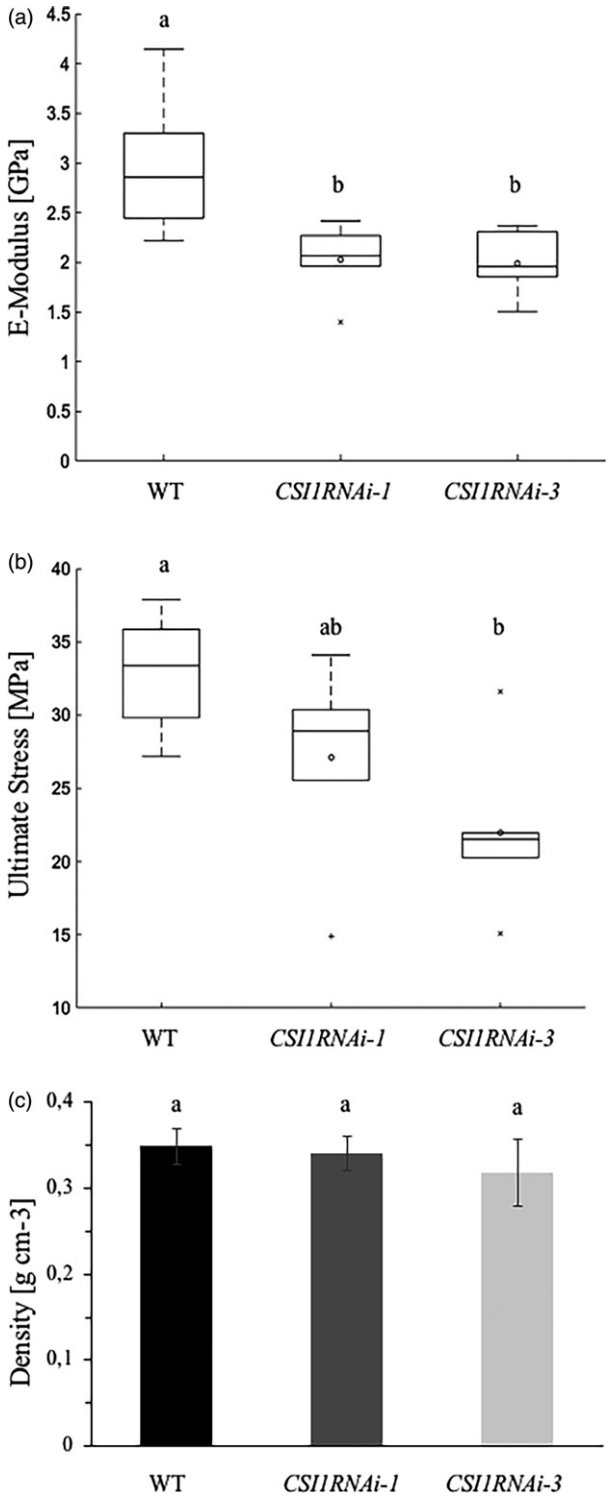

Figure 4. Mechanical properties of wild-type (WT) and *CSI1RNAi* hybrid aspen (*Populus tremula* × *tremuloides*) wood.
(a) Modulus of elasticity (b) modulus of rupture (c) density. Error bars represent ± SD ($n = 5$ (WT and *CSI1RNAi-1*) and $n = 6$ (*CSI1RNAi-3*) biological replicates.
Means not sharing a common letter are significantly different at $P < 0.05$, as determined by Tukey's test after one-way ANOVA.

Table 2 Wood cellulose microfibril angle (MFA) and macerated longitudinal fibre area in wild-type (WT) and *CSI1RNAi* hybrid aspen (*Populus tremula* × *tremuloides*) lines

	Average cellulose MFA (°)		
Line	Normal wood	Tension wood	Fibre area (μm^2)
WT	17.9 ± 2.7^a	5.5 ± 0.07^a	9655 ± 651^a
CSI1RNAi-1	16.4 ± 1.8^a	5.7 ± 0.4^a	7810 ± 314^b
CSI1RNAi-3	20.7 ± 4.4^a	4.8 ± 0.7^a	7409 ± 579^b

X-ray diffraction determined average MFA: Mean ± SD. Normal wood: WT and *CSI1RNAi-1* five trees and *CSI1RNAi-3* six trees, three to 10 wood sections per tree. Tension wood: WT two trees, *CSI1RNAi-1* five trees and *CSI1RNAi-3* three trees, one to nine wood sections per tree. Fibre area and fibre-tip length: mean ± SD, $n = 5$ (WT and *CSI1RNAi-1* and *CSI1RNAi-3*); molecular weight of cellulose: mean ± SD, $n = 4$–5 (WT and *CSI1RNAi-1 and CSI1RNAi-3*).
Means not sharing a common letter are significantly different at $P < 0.05$, as determined by Tukey's test after one-way ANOVA.

xylem fibres. Intriguingly, wood density as assessed in the same samples as used for the mechanical testing, was not changed (Figure 4c).

In addition to guiding the CSCs along the MTs, CSI1 mutations have been shown to reduce the average speed of CSCs in the plasma membrane in Arabidopsis (Gu *et al.*, 2010). A similar slowdown of CSCs during wood formation could lead to shorter cellulose chains if the lifetime of the CSCs at the plasma membrane does not change. To compare the degree of cellulose polymerization between WT and *CSI1RNAi* lines, cellulose was extracted from stem wood using peracetic acid (PAA) extraction. PAA is effective for lignin removal while minimizing the impact on CMF degradation (Poljak, 1948; Kumar *et al.*, 2013). After the PAA extraction and solvent exchange cellulose was dissolved in a lithium chloride/*N,N*-dimethylacetamide (LiCl/DMAc) solution, which is a non-degrading solvent for cellulose (Potthast *et al.*, 2015). To measure the absolute molecular weight of the cellulose fraction we used size exclusion chromatography (SEC) coupled to a laser light scattering (LS) detector, which allows the direct measurement of the molecular weight of polymers in solution (Einstein, 1910; Wyatt, 1993; Podzimek, 1994). The SEC/LS data indicated a slight decrease in the number average molar mass (M_n) and particularly in the weight average molar mass (M_w) of cellulose in the *CSI1RNAi* lines (Table 2.) The M_n values are the arithmetic average molecular weight of all cellulose molecules, whereas the M_w is the mass averaged molecular weight $\left(M_w = \frac{\sum M_i^2 n_i}{\sum M_i N_i}\right)$. Thus, M_w is more sensitive than M_n to decreases in the amount of the higher molecular weight cellulose molecules. This shift in the molecular weight distribution of CMFs is best illustrated by

comparing the SEC/LS graph of WT and the *CSI1RNAi* line 3 (Figure 5a). The M_w and M_n values were not significantly different between WT and transgenics (Table S3). However, a multivariate analysis using orthogonal projections to latent structures discriminant analysis (OPLS-DA) showed that the cellulose degree of polymerization (DP) in line 3 is significantly different from WT, while line 1 lies between the two (Figure 5b). OPLS-DA is suitable for determining the difference between groups (Bylesjö *et al.*, 2006). The horizontal component of the OPLS-DA score scatter plot shows the variation between the genotypes while the vertical dimension captures within genotype variation. The reduction in molecular weight distribution correlated with the reduction in ultimate stress in lines 1 and 3. These results support a role for CSI1 in defining the cellulose DP in wood, and represent a structural change associated with the mechanical phenotype.

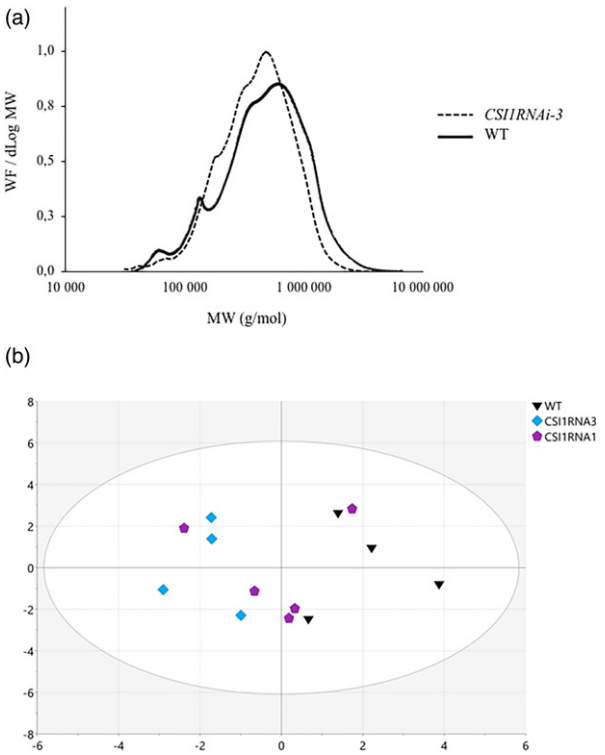

Figure 5. Size exclusion chromatogram analysis of wild-type (WT) and *CSI1RNAi* hybrid aspen (*Populus tremula* × *tremuloides*) stem wood cellulose.
(a) Molecular weight distribution of cellulose from WT and *CSI1RNAi* line 3.
(b) Molecular weight distribution of cellulose analysed using orthogonal projections to latent structures discriminant analysis (OPLS-DA). Scores plot shows the separation between WT (triangles) and *CSI1RNAi* line 1 (pentagons) and line 3 (squares). Each symbol represents one replicate tree. OPLS-DA R2X (cum) 0.82. Weight fraction (WF), derivative of logarithmic molecular weight (dLog MW).

DISCUSSION

Molecular mechanisms defining the mechanical properties of wood are poorly understood. The mechanical properties derive from cellular and molecular interactions at tissue and cell wall level. CMFs are the main load-bearing and tension resisting components in the cell walls. CSI1 was identified in Arabidopsis as a linker between cortical MTs and CSC with a role in guiding cellulose biosynthesis in the primary cell walls. We identified functional orthologues of CSI1 in aspen and show that they control the CMF length that, in turn, impacts the mechanical properties of the wood. In the developing wood of aspen *CSI1A* and *CSI1B* are expressed during primary cell wall biosynthesis and cell expansion as well as secondary cell wall formation (Figure 1). Reduction of *CSI1A* and *CSI1B* transcript level in the leaves to 50%–20% of WT resulted in leaves that twisted, likely due to the defects in pavement cell expansion and consequently cell shape (Figure 1). This is fitting with the results from Arabidopsis showing that the leaf pavement cell shape depends on cortical MT-dependent wall reinforcements in the neck regions of the cells (Fu *et al.*, 2005). Live imaging of fluorescently labelled MT has shown that the cortical MTs align along the maximal tensile stress, which then regulates pavement cell shape by controlling cellulose biosynthesis (Sampathkumar *et al.*, 2014). Hence, the leaf results of the *CSI1RNAi* lines suggest that CSI1 is involved in guiding CSCs in the pavement cells and consequently the directional cell expansion and leaf growth in aspen.

Wood growth is mainly radial, while primary growth typically expands in three directions at the same time. The mechanical forces shaping primary growth and epidermal cell walls differ from forces in developing wood, which grows against the pressure established by the phloem tissues (including bark). It is also worth noting that the secondary cell wall layers of xylem fibres and vessels are formed before the stresses they experience after maturation and cell death. Hence, the patterns in xylem secondary cell walls appear genetically hardwired and less plastic than in the primary walls. An example of this developmental cell wall pattern program is seen in suspension-cultured plant cells, which can be induced to form protoxylem vessels in the absence of any tissue-derived mechanical signals (Fukuda, 1996). The differences between primary and secondary cell wall growth suggests that the mechanosensing processes guiding primary cell wall cellulose biosynthesis may not explain CMF patterning in secondary cell walls. The reduction of *CSI1A* and *CSI1B* transcript abundance in the developing wood of the *CSI1RNAi* lines was shown to be 10%–30% of WT (Figure 1), and effectively allowed us to test the functional role of CSI1-mediated CSC guiding during wood formation and secondary growth in aspen. In the developing wood *CSI1A* and *CSI1B* transcript levels are abundant after cell expansion, suggesting a functional role in secondary cell wall formation (Figure 1). In support of this, the *CSI1RNAi* stem sections

were more brittle perpendicular to the direction of the fibre (Figure 3), and mechanically weaker in the longitudinal direction (Figure 4). We observed no significant differences in the chemical composition of wood or wood density that could explain the mechanical weakness (Figure 4 and Table S2). The fibre cells were approximately 20% smaller in the *CSI1RNAi* lines (Table 2). The reduced fibre area points to a defect in fibre cell expansion in agreement with the pavement cell defects in leaves and published results from Arabidopsis *csi1* mutants (Gu *et al.*, 2010). However, a correlation with the *CSI1RNAi* fibre size and the mechanical phenotype cannot currently be substantiated in the literature, as mechanical changes associated with wood fibre size change typically also coincide with other changes such as density and cell wall chemistry.

CMFs are the main load-bearing elements in the longitudinal direction, and based on the CSI1 function in CMF alignment during primary wall biosynthesis, we hypothesized a *CSI1RNAi* effect on MFA in wood. Experiments with both wood and isolated fibre samples have shown that the changes in the S_2 MFA correlate with changes in the resistance to tensile stress and elastic deformation of the fibre wall or woody tissue (Preston, 1974). We used X-ray diffraction to measure the average MFA in the S_2 layer of fibre walls and in areas showing characteristics of a typical tension wood G-layer MFA angle. These measurements did not reveal consistent differences in the average MFA of *CSI1RNAi* and WT (Table 2). The MFA in the tension wood S_2 layer is similar or higher compared with normal wood S_2, while in the G-layer the MFA in the same cells changes to near parallel to the fibre axis (Clair *et al.*, 2010). Hence, the lack of a MFA phenotype in *CSI1RNAi* G-layers suggests that CSI1 is not involved in the dynamic secondary cell wall MFA response to mechanical and gravity cues (Table 2). The lack of MFA phenotype in the *CSI1RNAi* trees is in line with the Arabidopsis results showing that CSI1 is not needed for the maintenance of the CMF pattern in xylem vessels (Schneider *et al.*, 2017). We cannot exclude the possibility that the *CSI1RNAi* lines still contained sufficient residual CSI1 activity during secondary cell wall formation. However, the transcript levels in developing wood were reduced more than in the twisting leaves providing some support against remaining CSI1 activity as the reason for no apparent MFA phenotype in wood.

We discovered a shift in the cellulose DP distribution towards shorter CMFs in the transgenics (Figure 5). The reduction in cellulose DP could manifest from one of several possibilities, including but not limited to, *CSI1RNAi* reduced half-life of CSCs in the plasma membrane and/or reduced rate of cellulose biosynthesis. The latter possibility is supported by experiments in Arabidopsis showing reduced velocity of YFP-CESA6 particles in the hypocotyls of *csi1* mutants (Gu *et al.*, 2010; Lei *et al.*, 2013). In a subsequent study, Lei *et al.* (2015) showed that CSI1 is also involved in the formation of endocytosis-derived CSC containing vesicles in the vicinity of the plasma membrane. Thus, it is possible that CSC endocytosis defects in the *CSI1RNAi* could cause shortening of the CMFs. We hypothesize that CMF length contributes to the mechanical strength of wood, and that the reduction in cellulose DP contributed towards the mechanical wood phenotype. Interestingly, the reduction in cellulose DP and MOR in longitudinal fibre direction appeared linked (Figures 4b and 5b) indicating that the length of the cellulosic glucan chains increases the strength of wood. However, it is important to note that any kind of chemical treatment and extraction is likely to decrease the cellulose DP. Hence we cannot exclude the possibility that the *CSI1RNAi* cellulose DP is equal to WT *in situ*, but the CMFs have structural defects making them more sensitive than WT microfibrils to the PAA extraction and LiCl/DMAc solubilization. Despite the analytical limitations in the SEC-LS procedure, it can be concluded that *CSI1RNAi* affects cellulose biosynthesis in wood. We hypothesize that *CSI1RNAi* caused reduced cellulose DP and/or structural changes in the CMFs, which may affect CMF interaction with the other matrix components, thereby contributing to weakening of the wood. To dissect the aspen CSI1 function further it will be informative to create *CSI1* null mutants using the CRISPR genome editing technology.

EXPERIMENTAL PROCEDURES

Plant material and growth conditions

Transgenic and WT hybrid aspen (*Populus tremula* × *tremuloides*) trees were micropropagated *in vitro* for 4 weeks and then transferred to the greenhouse for further growth in commercial soil and fertilizer mixture (Hasselfors Garden Planteringsjord, https://www.hasselforsgarden.se) under an 18-h light/6-h dark photoperiod at a temperature of 22°C/15°C (light/dark) and 50%–70% humidity. The trees were fertilized using 150 ml 1% Rika-S (N/P/K, 7:1:5; Weibulls Horto, SW Horto AB, Hammenhög, Sweden) once a week for the first 3 weeks of greenhouse growth.

The trees were harvested after 8 weeks of growth in the greenhouse. Stem diameter was measured 10 cm above the soil using digital calipers, while stem height was determined as the distance between the soil surface and the shoot tip. Wood samples for gene expression analysis, wood anatomy, wood chemistry and mechanical tests were collected from a stem section 10–60 cm above the soil. Samples for gene expression analysis were immediately frozen in liquid nitrogen, while the samples for chemistry and mechanical tests were placed on dry ice and stored at −80°C. Stem wood anatomy sections were prepared from material (stored at −80°C until use) cut 10 cm above the soil, while samples used for fibre maceration and cellulose degree of polymerization analysis originated from 40 to 50 cm above soil and were dried and stored at room temperature until use. Fully expanded leaves for transcript abundance analysis were collected, frozen in liquid nitrogen and stored at −80°C until use. The area of fully expanded leaves was determined using a LI-3000C Portable Leaf Area Meter (LI-COR Bioscience,

www.licor.com) on the leaf number 17, counting down from the first fully emerged leaf at the top of the tree.

CSI1RNAi vector construction, hybrid aspen transformation and qPCR

The RNA interference cassette was created in the pBluescript SK+ vector using a 171-bp fragment targeting *PtCSI1A* (Potri.007G087200) and *PtCS1B* (Potri.005G080100). Hybrid aspen was transformed as described by Nilsson *et al*. (1992). Quantitative real-time PCR was used to determine Pt*CSI1A* and Pt*CSI1B* transcript abundance. *UBIQUITIN* transcript abundance was used as a reference gene. Primers for *PtCSI1A* and *PtCSI1B* are listed in Table S1.

Complementation of Arabidopsis *pom2-4*

Total RNA extracted from *Populus tremula* × *tremuloides* wood was transcribed into cDNA using SuperScript™ III Reverse Transcriptase Kit. *CSI1A* coding sequence (6456 bp) was PCR amplified from the corresponding cDNA using Phusion High-Fidility DNA polymerase (Thermo Fisher Scientific, www.thermofisher.com) with primers specifically containing Gibson cloning sequence (Table S1) and cloned into Gateway entry vector pDONR207 using HiFi DNA Assembly cloning Kit (E5520S; New England Biolabs, www.neb.uk.com) following the manufacturer's instructions. The presence of the *CSI1A* sequence was confirmed by sequencing and then recombined into the destination vector pH2GW7 using Gateway LR Clonase Enzyme mix (Thermo Fisher Scientific). The *CSI1A* construct, under the control of the 35S promoter, was introduced into the Arabidopsis *pom2-4* mutant by *Agrobacterium tumefaciens* using the floral dipping method (Clough and Bent, 1998). Transgenic lines were selected on agar plates containing hygromycin (25 mg/L), and homozygous lines were selected in the T2 generation. The incorporation of the *CSI1A* sequence into the *pom2-4* genomic DNA was confirmed by genomic PCR.

Gene expression analysis

Leaves and developing wood scrapings were homogenized in liquid nitrogen using a mortar and pestle. Total RNA was isolated using TRIZOL® Reagent. In short, 5 μg of total RNA was transcribed into cDNA and amplified using a Maxima First Strand cDNA Synthesis Kit containing dsDNase (Thermo Scientific). qPCR was performed using a CFX96™ Real-Time System (C1000™ Thermal Cycler; Bio-Rad, http://www.bio-rad.com/) and double-stranded DNA was detected using iQTM SYBR® Green Supermix (Bio-Rad). UBIQUITIN transcript levels were used as a reference for developing wood and leaf samples. Relative transcript level was calculated using the Bio-Rad CFX Manager Software. Gene-specific primers are listed in Table S1.

Wood anatomy

For light microscopy, 20-μm thick wood cross-sections were prepared using a cryotome (−20°C). The sections were stained with safranin/alcian blue and visualized using a Leica DMLB light microscope and a Leica DC300 camera (www.leicamicrosystems.com). For TEM imaging, 200-μm thick cross-sections were fixed overnight in 2.5% (w/v) glutaraldehyde/0.1 cacodylate buffer (pH 7.4). Then the sections were washed twice with cacodylate buffer and transferred to a 1% (w/v) osmium tetroxide solution for 2 h in the dark. After washing twice for 15 min in 0.1 M cacodylate buffer, the wood sections were dehydrated via an ethanol dilution series and finally transferred to a mix of anhydrous ethanol and Spurr embedding resin (TAAB Laboratories, Aldermaston, UK) and embedded in beem capsules and incubated at 65°C for 24 h. After embedding, ultrathin sections of 80 nm thickness were cut for TEM analysis. The sections were stained with 5% aqueous uranyl acetate for 60 min and then with lead citrate (Reynolds, 1963) for 6 min before examination with TEM (JEM 1230; JEOL, Tokyo, Japan). Pictures were taken using a GAtan MSC 600CW 2k × 2k CCD camera.

Wet chemical analysis of wood

Cell wall chemical composition of WT and transgenic trees was measured using a subsample of isolated stem sections. Cell wall carbohydrates and total lignin were measured by first grinding the solid xylem tissue in a Wiley Mill to pass a 40 mesh and then extracted with hot acetone in Soxhlet apparatus for a minimum of 12 h. Cell wall carbohydrates and total lignin (acid-soluble and -insoluble lignin, in combination forming total lignin) were determined as described in Huntley *et al*. (2003) using a modified Klason method. Cell wall carbohydrates were quantified with a high-performance liquid chromatography system using a DX-600 (Dionex, Sunnyvale, CA, USA) equipped with a PA1 (Dionex) column, detector with a gold electrode and SpectraAS3500 auto injector (Spectra-Physics, Santa Clara, CA, USA). Carbohydrate amounts were quantified relative to monomeric cell wall-associated carbohydrates (glucose, xylose, mannose, galactose, rhamnose and arabinose). The amounts of Klason lignin and cell wall sugars represent percentages, relative to the initial weight of dry wood sample analysed.

Mechanical tests

Mechanical properties of the wood specimens were measured using a microtensile testing stage described by Burgert *et al*. (2003). The samples were prepared from specimens isolated 10–20 cm above soil. Longitudinal sections were prepared using a scalpel to obtain a wood block of approximately 25 × 2 × 0.1 mm (length × width × thickness). Tangential longitudinal sections of 100 μm thickness were then cut using a cryotome at −20°C. The cambium region was first removed, and then 10 consecutive longitudinal tangential sections were cut and considered as technical replicates and stored in double-distilled (dd)H_2O until physical testing. The values of the technical replicates were used to calculate the mean of the biological replicates. Strain measurement was performed with video extensometry using a stereomicroscope and a CCD camera. The test length was set to 12 mm and the samples were subjected to a constant strain of 10 μm sec^{-1}. The force was recorded with a 50-N load cell (Sensotec Sensors, Honeywell, http://www.honeywell.com). Wood density was determined on the same wood samples as used for the mechanical tests. Density was measured based on wet volume (length, width and thickness) and air dried (48 h at room temperature) weight, using the formula P = m/V.

MFA

CMF angles were determined by measuring CMF orientation of all mechanically tested specimens by wide-angle X-ray diffraction. A Nanostar (Bruker AXS, Ettlingen, Germany) was used equipped with a 2D detector (HySitron, www.bruker.com) and a CuKα radiation source with a wavelength of 0.154 nm. The X-ray beam diameter was set to about 300 μm and the sample–detector distance was set to 8.5 cm. For each sample, one diffraction image was taken with 800-sec exposure time. From the diffraction images, azimuthal intensity profiles of the (200)-Bragg peak of cellulose were calculated with a step size of 1° by radial integrating the intensity within the *q*-range of the (200)-Bragg peak. The

contribution of the amorphous part of cellulose was subtracted from this profile as an azimuthal intensity profile integrated within a short *q*-range at slightly larger *q* values next to the (200)-Bragg peak. Simulated azimuthal intensity profiles were then fitted to the measured profiles, which revealed mean and deviation values for each measuring spot assuming a superposition of two Gaussian distributions according to Rüggeberg *et al.* (2013). For the simulation of the azimuthal intensity profile, a representative cell wall orientation profile is taken from a sample cross-section. Technical replicates in which tension wood was found were omitted from statistical analysis of normal wood MFA.

Cellulose degree of polymerization

The molecular weight distribution of the cellulose fraction was analysed using SEC coupled to a LS detector. Samples were prepared from air-dried stems using a coarse wood rasp file to minimize the effect on CMFs. Lignin was removed by a method described in Kumar *et al.* (2013). Briefly, 0.5 g (5% solids) of the wood powder was suspended in 2.625 g ddH_2O and 6.875 g 38%–40% PAA and incubated for 48 h at room temperature under constant shaking. Samples were then treated in 18% (w/w) NaOH for 2 min at room temperature to dissolve hemicellulose. After this, the samples were washed with ddH_2O until a neutral pH was achieved and then vacuum filtrated. Approximately 25 mg (dry weight) of cellulose was solvent exchanged to methanol in three steps and subsequently to DMAc in three steps. The samples were then fully dissolved in 8% LiCl/DMAc overnight under shaking. The samples were finally diluted to a concentration of 1 mg ml^{-1} for measurements. The SEC system (Omnisec resolve from Malvern, www.malvernpanalytical.com) consisted of a guard column and two serial T6000M columns from Malvern. The autosampler temperature was set at 50°C and the column and the detector ovens at 60°C. The eluent contained DMAc with 1% LiCl and the flow rate was 0.5 ml min^{-1}. The detector system was a Malvern instruments Omnisec Reveal containing a refractive index, a viscometer (DP), a laser light scattering (low-angle LS, right-angle LS) and a multi-angle laser LS detector. The system was calibrated using a broad and a narrow poly(methylmethacrylate) standard (PolyCAL™ PMMA Std-PMMA-60K, narrow standard: M_w = 59 575 g mol^{-1}, M_n = 56 512; broad standard: M_w = 94 986 g mol^{-1}, M_n 47 198). The data were evaluated with the OMNISEC V10 software from Malvern.

Multivariate data analysis

The SEC data were examined using multivariate data analysis. All calculations were done with the software Simca 16 (Umetrics, Sweden). A model was created as an OPLS-DA, with WT, line 1 and line 3 as three separate classes and with all variables treated as 'X variables' (Bylesjo *et al.*, 2006). These variables were the position of the refractive index, DP, multi-angle laser LS, right-angle LS and low-angle LS peaks (eluted volume of solvent) and the calculated values (from Omnisec 10) of the M_w, M_n, M_w/M_n, and intrinsic viscosity. Unit variance scaling was used.

Xylem fibre area measurements

Air-dried wood specimens were cut in small pieces of 2–3 mm thickness and approximately 1 cm in length. The wood pieces were then incubated for 12 h at 95°C in 50% acetic acid and 3% of H_2O_2. The maceration solution was removed and samples washed with water two times. A few milligrams of sodium carbonate were added to neutralize the acetic acid and then samples were washed with water at two subsequent times. Fibre images were recorded using a Zeiss Axioplan2 light microscope and a Zeiss AxioCam HRC Camera (www.ZEISS.com). The fibre area was measured from the images using IMAGEJ software (http://rsbweb.nih.gov).

ACCESSION NUMBERS

Sequence data from this article can be found in Popgenie.org *Populus trichocarpa* genome sequence version 3.0 under the following gene identification numbers: Potri.007G087200 (*PtCSl1A*) and Potri.005G080100 (*PtCSl1B*).

ACKNOWLEDGEMENTS

We thank Cheng Choo Lee and Agnieszka Ziolkowska for assistance with electron microscopy, Junko Takahashi-Schmidt and the biopolymer analytical facility at UPSC for help with wood analysis and Valentina Floran for help with the cloning of the CSI1RNAi construct. This work was supported by Bio4Energy (Swedish Programme for Renewable Energy), the Umeå Plant Science Centre, Berzelii Centre for Forest Biotechnology funded by VINNOVA and the Swedish Research Council for Sustainable Development (Formas). Staffan Persson was supported by R@MAP Professor Funds at University of Melbourne and ARC DP and FT grants (DP190101941; FT160100218).

AUTHOR CONTRIBUTIONS

AB, OS, AM and MR planned and performed experiments and analysed data. TN, SM and SP planned experiments and analysed data. AB, OS, AM, MR, SM, SP and TN wrote the manuscript.

CONFLICT OF INTEREST

The authors declare that they have no competing interests.

DATA AVAILABILITY STATEMENT

All data are contained within the manuscript. All materials used in the study will be available upon request.

SUPPORTING INFORMATION

Additional Supporting Information may be found in the online version of this article.

Figure S1. Alignment of *Populus* CSl1A and CSl1B amino acid sequences.

Figure S2. Arabidopsis *pom2-4* complementation using *Populus CSl1A*.

Table S1. Primer and the RNAi sequences.

Table S2. Wood chemistry analysis.

Table S3. Cellulose molar mass averages.

REFERENCES

Bailey, I.W. and Vestal, M.R. (1937) The orientation of cellulose in the secondary wall of tracheary cells. *J. Arnold. Arbor.* **18**, 185–195.

Barnett, J.R. and Bonham, V.A. (2004) Cellulose microfibril angle in the cell wall of wood fibres. *Biol. Rev.* **79**, 461–472.

Beery, W., Ifju, G. and McLain, T. (1983) Quantitative wood anatomy–relating anatomy to transverse tensile strength. *Wood Fiber Sci.* **15**, 395–407.

Bringmann, M., Landrein, B., Schudoma, C., Hamant, O., Hauser, M.-T. and Persson, S. (2012a) Cracking the elusive alignment hypothesis: the

microtubule–cellulose synthase nexus unraveled. *Trends Plant Sci.* **17**, 666–674.

Bringmann, M., Li, E., Sampathkumar, A., Kocabek, T., Hauser, M.T. and Persson, S. (2012b) POM-POM2/cellulose synthase interacting1 is essential for the functional association of cellulose synthase and microtubules in Arabidopsis. *Plant Cell*, **24**, 163–177.

Burgert, I., Frühmann, K., Keckes, J., Fratzl, P. and Stanzl-Tschegg, S.E. (2003) Microtensile testing of wood fibers combined with video extensometry for efficient strain detection. *Holzforschung*, **57**, 661–664.

Bylesjo, M., Rantalainen, M., Cloarec, O., Nicholson, J.K., Holmes, E. and Trygg, J. (2006) OPLS discriminant analysis: combining the strengths of PLS-DA and SIMCA classification. *J. Chemometr.* **20**, 341–351.

Bylesjö, M., Rantalainen, M., Cloarec, O., Nicholson, J.K., Holmes, E. and Trygg, J. (2006) OPLS discriminant analysis: combining the strengths of PLS-DA and SIMCA classification. *J Chemom.* **20**, 341–351.

Chaffey, N., Barlow, P. and Barnett, J. (2000) A cytoskeletal basis for wood formation in angiosperm trees: the involvement of microfilaments. *Planta*, **210**, 890–896.

Chaffey, N., Barlow, P. and Sundberg, B. (2002) Understanding the role of the cytoskeleton in wood formation in angiosperm trees: hybrid aspen (*Populus tremula* × *P. tremuloides*) as the model species. *Tree Physiol.* **22**, 239–249.

Clair, B., Alméras, T., Pilate, G., Jullien, D., Sugiyama, J. and Riekel, C. (2010) Maturation stress generation in poplar tension wood studied by synchrotron radiation microdiffraction. *Plant Physiol.* **152**, 1650–1658.

Clough, S.J. and Bent, A.F. (1998) Floral dip: a simplified method for Agrobacterium-mediated transformation of *Arabidopsis thaliana*. *Plant J.* **16**, 735–743.

Cosgrove, D.J. (2005) Growth of the plant cell wall. *Nat. Rev. Mol. Cell Biol.* **6**, 850.

Einstein, A. (1910) Theorie der Opaleszenz von homogenen Flüssigkeiten und Flüssigkeitsgemischen in der Nähe des kritischen Zustandes. *Ann. Phys.* **338**, 1275–1298.

Evans, R. and Elic, J. (2001) Rapid prediction of wood stiffness from microfibril angle and density. *Forest. Prod. J.* **51**(3), 53.

Fengel, D. and Stoll, M. (1973) Über die Veränderungen des Zellquerschnitts, der Dicke der Zellwand und der Wandschichten von Fichtenholz-Tracheiden innerhalb eines Jahrringes. *Holzforschung*, **27**, 1–7.

Fengel, D., Wegener, G. and Greune, A. (1989) Studies on the delignification of spruce wood by organosolv pulping using SEM-EDXA and TEM. *Wood Sci. Technol.* **23**, 123–130.

Fu, Y., Gu, Y., Zheng, Z., Wasteneys, G. and Yang, Z. (2005) Arabidopsis interdigitating cell growth requires two antagonistic pathways with opposing action on cell morphogenesis. *Cell*, **120**, 687–700.

Fukuda, H. (1996) Xylogenesis: initiation, progression, and cell death. *Annu. Rev. Plant Biol.* **47**, 299–325.

Funada, R., Abe, H., Furusawa, O., Imaizumi, H., Fukazawa, K. and Ohtani, J. (1997) The orientation and localization of cortical microtubules in differentiating conifer tracheids during cell expansion. *Plant Cell Physiol.* **38**, 210–212.

Gibson, E. (1992) Wood: a natural fibre reinforced composite. *Met. Mater.* **8**, 333–336.

Gorshkova, T., Brutch, N., Chabbert, B., Deyholos, M., Hayashi, T., Lev-Yadun, S., Mellerowicz, E.J., Morvan, C., Neutelings, G. and Pilate, G. (2012) Plant fiber formation: state of the art, recent and expected progress, and open questions. *Crit. Rev. Plant Sci.* **31**, 201–228.

Groover, A.T., Nieminen, K., Helariutta, Y. and Mansfield, S.D. (2010) Wood formation in Populus. In *Genetics and genomics of Populus*. New York, NY: Springer. pp. 201–224.

Gu, Y., Kaplinsky, N., Bringmann, M., Cobb, A., Carroll, A., Sampathkumar, A., Baskin, T.I., Persson, S. and Somerville, C.R. (2010) Identification of a cellulose synthase-associated protein required for cellulose biosynthesis. *Proc. Natl. Acad. Sci. USA*, **107**, 12866–12871.

Gu, Y. and Somerville, C. (2010) Cellulose synthase interacting protein: a new factor in cellulose synthesis. *Plant Signal Behav.* **5**, 1571–1574.

Harada, H. (1962) Electron microscopy of ultrathin sections of beech wood (Fagus crenata Blume). *J. Japan Wood Res. Soc.* **8**, 252–258.

Huntley, S.K., Ellis, D., Gilbert, M., Chapple, C. and Mansfield, S.D. (2003) Significant increases in pulping efficiency in C4H–F5H-transformed poplars: improved chemical savings and reduced environmental toxins. *J Agric Food Chem.* **51**, 6178–6183.

Kerr, T. and Bailey, I.W. (1934) The cambium and its derivative tissues: No. X. Structure, optical properties and chemical composition of the so-called middle lamella. *J. Arnold. Arbor.* **15**, 327–349.

Kumar, R., Hu, F., Hubbell, C.A., Ragauskas, A.J. and Wyman, C.E. (2013) Comparison of laboratory delignification methods, their selectivity, and impacts on physiochemical characteristics of cellulosic biomass. *Biores. Technol.* **130**, 372–381.

Landrein, B., Lathe, R., Bringmann, M., Vouillot, C., Ivakov, A., Boudaoud, A., Persson, S. and Hamant, O. (2013) Impaired cellulose synthase guidance leads to stem torsion and twists phyllotactic patterns in Arabidopsis. *Curr. Biol.* **23**, 895–900.

Lei, L., Li, S., Du, J., Bashline, L. and Gu, Y. (2013) Cellulose synthase INTERACTIVE3 regulates cellulose biosynthesis in both a microtubule-dependent and microtubule-independent manner in Arabidopsis. *Plant Cell*, **25**, 4912–4923.

Lei, L., Singh, A., Bashline, L., Li, S., Yingling, Y.G. and Gu, Y. (2015) CELLULOSE SYNTHASE INTERACTIVE1 is required for fast recycling of cellulose synthase complexes to the plasma membrane in Arabidopsis. *Plant Cell*, **27**(10), 2926–2940. https://doi.org/10.1105/tpc.15.00442

Li, S., Bashline, L., Zheng, Y., Xin, X., Huang, S., Kong, Z., Kim, S.H., Cosgrove, D.J. and Gu, Y. (2016) Cellulose synthase complexes act in a concerted fashion to synthesize highly aggregated cellulose in secondary cell walls of plants. *Proc. Natl Acad. Sci. USA*, **113**, 11348–11353.

Li, S., Lei, L., Somerville, C.R. and Gu, Y. (2012) Cellulose synthase interactive protein 1 (CSI1) links microtubules and cellulose synthase complexes. *Proc. Natl Acad. Sci. USA*, **109**, 185–190.

Müller, M., Burghammer, M. and Sugiyama, J. (2006) Direct investigation of the structural properties of tension wood cellulose microfibrils using microbeam X-ray fibre diffraction. *Holzforschung*, **60**(5), 474–479.

Nilsson, O., Alden, T., Sitbon, F., Anthony Little, C.H., Chalupa, V., Sandberg, G. and Olsson, O. (1992) Spatial pattern of cauliflower mosaic virus 35S promoter-luciferase expression in transgenic hybrid aspen trees monitored by enzymatic assay and non-destructive imaging. *Transgenic Res.* **1**, 209–220.

Oda, Y., Mimura, T. and Hasezawa, S. (2005) Regulation of secondary cell wall development by cortical microtubules during tracheary element differentiation in Arabidopsis cell suspensions. *Plant Physiol.* **137**, 1027–1036.

Paredez, A.R., Somerville, C.R. and Ehrhardt, D.W. (2006) Visualization of cellulose synthase demonstrates functional association with microtubules. *Science*, **312**, 1491–1495.

Podzimek, S. (1994) The use of GPC coupled with a multiangle laser light scattering photometer for the characterization of polymers. On the determination of molecular weight, size and branching. *J. Appl. Polym. Sci.* **54**, 91–103.

Poljak, A. (1948) Holzaufschluss mit Peressigsäure. *Angew. Chem.* **60**, 45–46.

Potthast, A., Radosta, S., Saake, B., Lebioda, S., Heinze, T., Henniges, U., Isogai, A., Koschella, A., Kosma, P. and Rosenau, T. (2015) Comparison testing of methods for gel permeation chromatography of cellulose: coming closer to a standard protocol. *Cellulose*, **22**, 1591–1613.

Preston, R.D. (1974) *The Physical Biology of Plant Cell Walls*. London: Chapman & Hall.

Reiterer, A., Lichtenegger, H., Fratzl, P. and Stanzl-Tschegg, S. (2001) Deformation and energy absorption of wood cell walls with different nanostructure under tensile loading. *J. Mater. Sci.* **36**, 4681–4686.

Reynolds, E.S. (1963) The use of lead citrate at high pH as an electron-opaque stain in electron microscopy. *J. Cell. Biol.* **17**, 208.

Roberts, A., Frost, A., Roberts, E. and Haigler, C. (2004) Roles of microtubules and cellulose microfibril assembly in the localization of secondary-cell-wall deposition in developing tracheary elements. *Protoplasma*, **224**, 217–229.

Rüggeberg, M., Saxe, F., Metzger, T.H., Sundberg, B., Fratzl, P. and Burgert, I. (2013) Enhanced cellulose orientation analysis in complex model plant tissues. *J. Struct. Biol.* **183**, 419–428.

Sampathkumar, A., Krupinski, P., Wightman, R., Milani, P., Berquand, A., Boudaoud, A., Hamant, O., Jönsson, H. and Meyerowitz, E.M. (2014) Subcellular and supracellular mechanical stress prescribes cytoskeleton behavior in Arabidopsis cotyledon pavement cells. *Elife*, **3**, e01967.

Schneider, R., Tang, L., Lampugnani, E.R., Barkwill, S., Lathe, R., Zhang, Y., McFarlane, H.E., Pesquet, E., Niittyla, T. and Mansfield, S.D. (2017) Two complementary mechanisms underpin cell wall patterning during xylem vessel development. *Plant Cell*, **29**, 2433–2449.

Watanabe, Y., Meents, M., McDonnell, L., Barkwill, S., Sampathkumar, A., Cartwright, H., Demura, T., Ehrhardt, D., Samuels, A. and Mansfield, S. (2015) Visualization of cellulose synthases in Arabidopsis secondary cell walls. *Science*, **350**, 198–203.

Watanabe, Y., Schneider, R., Barkwill, S., Gonzales-Vigil, E., Hill, J.L., Samuels, A.L., Persson, S. and Mansfield, S.D. (2018) Cellulose synthase complexes display distinct dynamic behaviors during xylem transdifferentiation. *Proc. Natl. Acad. Sci. USA*, **115**, E6366–E6374.

Wightman, R. and Turner, S.R. (2008) A novel mechanism important for the alignment of microtubules. *Plant Signal. Behav.* **3**, 238–239.

Wyatt, P.J. (1993) Light scattering and the absolute characterization of macromolecules. *Anal. Chim. Acta*, **272**, 1–40.